Raman Self-Frequency Shift of Dissipative Kerr Solitons in an Optical Microresonator

Maxim Karpov, Hairun Guo, Arne Kordts, Victor Brasch, Martin H. P. Pfeiffer, Michail Zervas, Michael Geiselmann, and Tobias J. Kippenberg*

École Polytechnique Fédérale de Lausanne (EPFL), CH-1015 Lausanne, Switzerland

(Received 2 July 2015; published 11 March 2016)

The formation of temporal dissipative Kerr solitons in microresonators driven by a continuous-wave laser enables the generation of coherent, broadband, and spectrally smooth optical frequency combs as well as femtosecond pulse sources with compact form factors. Here we report the observation of a Raman-induced soliton self-frequency shift for a microresonator dissipative Kerr soliton also referred to as the frequency-locked Raman soliton. In amorphous silicon nitride microresonator-based single soliton states the Raman effect manifests itself by a spectrum that is sech^2 in shape and whose center is spectrally redshifted from the continuous wave pump laser. The shift is theoretically described by the first-order shock term of the material's Raman response, and we infer a Raman shock time of ~20 fs for amorphous silicon nitride. Moreover, we observe that the Raman-induced frequency shift can lead to a cancellation or overcompensation of the soliton recoil caused by the formation of a coherent dispersive wave. The observations are in agreement with numerical simulations based on the Lugiato-Lefever equation with a Raman shock term. Our results contribute to the understanding of Kerr frequency combs in the soliton regime, enable one to substantially improve the accuracy of modeling, and are relevant to the understanding of the fundamental timing jitter of microresonator solitons.

DOI: 10.1103/PhysRevLett.116.103902

Introduction.—Microresonator-based optical frequency combs (Kerr combs) [1,2] enable optical frequency comb generation from a continuous wave (cw) laser with repetition rates in the microwave domain (>10 GHz) and broad spectral bandwidth [3–5], and have been used in proof-of-concept applications such as atomic clocks or coherent telecommunications [6,7]. Recently, a qualitatively new operation regime has been discovered [8], in which the parametrically generated comb seeds the formation of temporal dissipative Kerr solitons [9,10]. Such solitons have been discovered to spontaneously form in crystalline microresonators [8,11] and have recently also been generated in photonic-chip-based integrated silicon nitride (Si_3N_4) resonators [5,12], as well as in silica wedge resonators [12,13]. Soliton-based microresonator frequency combs (soliton combs) have several attractive features, in particular, being fully coherent, having smooth envelopes, and giving access to femtosecond pulses.

Indeed, femtosecond solitons in microresonators have intense peak power and ultrashort duration such that, in principle, they could excite higher-order nonlinear effects such as the self-steepening effect and intrapulse Raman scattering (IRS). The latter usually exists and is broadband in nature in amorphous materials such as silica and Si_3N_4, which relates to the vibrational material response of the cubic nonlinearity. Material Raman studies revealed typical active modes of, e.g., monosilicon bonds (520-cm^{-1} shift), silicon-oxygen bonds (450 cm^{-1}, broadband) [14], and silicon-nitrogen bonds (NSi_3 symmetric vibration mode, 380–430 cm^{-1}; Si-N-Si symmetric bending modes,

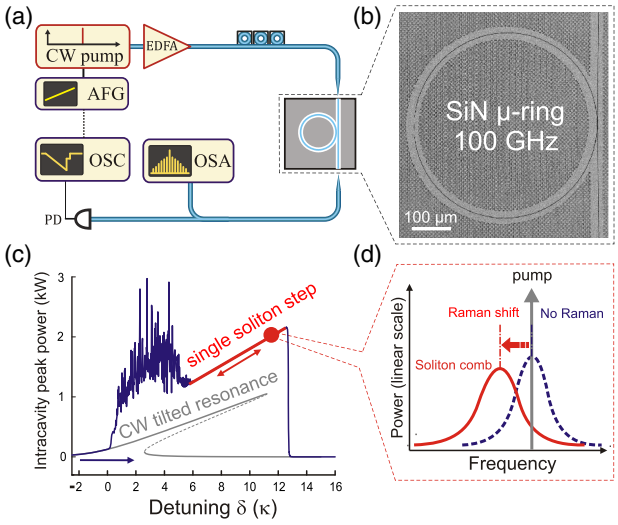

FIG. 1. (a) Diagram of the experimental setup: AFG, arbitrary function generator; EDFA, erbium-doped fiber amplifier; OSA, optical spectrum analyzer; OSC, oscilloscope; PD, photodiode. (b) SEM image of Si_3N_4 microresonator with a mode spacing of 100 GHz. (c) Illustration of the pump laser detuning excitation scheme (reducing the pump frequency). The gray line shows the Kerr-induced cw tilted resonance; the blue line shows the trace of intracavity peak power with an increase of the cavity resonance-pump detuning $2\pi\delta = \omega_0 - \omega_p$ (ω_0 and ω_p are the resonance and pump frequency); the red line shows the single soliton existence range. (d) Illustration of the Raman redshift on the frequency comb spectrum.

514 cm^{-1}) [15]. In silica fibers, IRS on ultrashort femtosecond pulses has been widely investigated [16,17] in the context of fiber-based supercontinuum generation and soliton propagation [18,19]. The observed phenomena include, among others, the soliton self-frequency shift that continuously shifts the whole pulse spectrum to the red wavelength side upon propagation [20–24], soliton fission when a higher-order soliton is split into fundamental solitons [25], and Raman-induced pulse compression in dispersive media [17]. While well studied in fiber, to date, however, the Raman effects in microresonator frequency combs (and more broadly for the class of dissipative Kerr solitons) has not been observed experimentally. The case of soliton formation in crystalline microresonators has not shown any evidence [8,11]. For amorphous silica- and Si_3N_4-based microresonators, the Raman effects were estimated by numerical simulations [26–28]. In particular, the work from Milián *et al.* [26] demonstrated that dissipative Kerr solitons can still form in the presence of the Raman effects [termed as *frequency-locked Raman (FLR) solitons*]. Simulations also predicted that a spectral redshift of a frequency comb can be induced when a stable soliton state is formed. In this Letter, we report for the first time, to our knowledge, the direct experimental observation of the Raman-induced soliton self-frequency shift in microresonators and investigate the Raman-induced soliton physics in microresonators that is distinct from the well-known fiber solitons [19].

Experiments.—The study is based on Si_3N_4 microresonators [5,29] in which, recently, dissipative Kerr solitons were generated [12]. The first set of samples was fabricated by a newly developed "photonic Damascene process" [30]. Samples have a free spectral range (FSR) $D_1/2\pi =$ 75–100 GHz for the fundamental TE mode family. Resonators have a nominal waveguide height of 0.9 μm and a width of 1.65 μm. The microresonator resonance linewidth near 1550 nm corresponds to $\kappa/2\pi \approx 200$ MHz (i.e., a quality factor $Q \approx 10^6$). Near 1550 nm, an anomalous group velocity dispersion parameter $D_2/2\pi =$ 1–2 MHz and a third-order dispersion $D_3/2\pi = \mathcal{O}(1)$ kHz are measured (whereby the resonance frequencies near the central mode ω_0 are expressed in a series $\omega_\mu = \omega_0 + \sum_{i\geq 1} D_i \mu^i / i!$, where $i \in \mathbb{N}$, $\mu \in \mathbb{Z}$ is the mode number).

Figure 1(a) shows the experimental setup. The cw pump is red-tuned to sweep over a resonance with constant speed (1 nm/s). The pump power is 1–3 W. As previously reported, transitions to dissipative-Kerr-soliton states can be identified from the power trace of the generated comb light [8] that shows a steplike pattern [e.g., Fig. 1(c)]. Stable multiple and single solitons are repeatedly achievable by properly stopping the laser tuning on such steps [8]. Typical single-soliton-based frequency combs are shown in Figs. 2(a)–2(c). The comb spectral envelope exhibits a symmetric and smooth $sech^2$ shape with a 3-dB bandwidth of ~5.5 THz, despite minor irregularities (e.g., the spike at 198.5 THz) caused by avoided mode crossing [11]. One striking difference to prior work in crystalline resonators

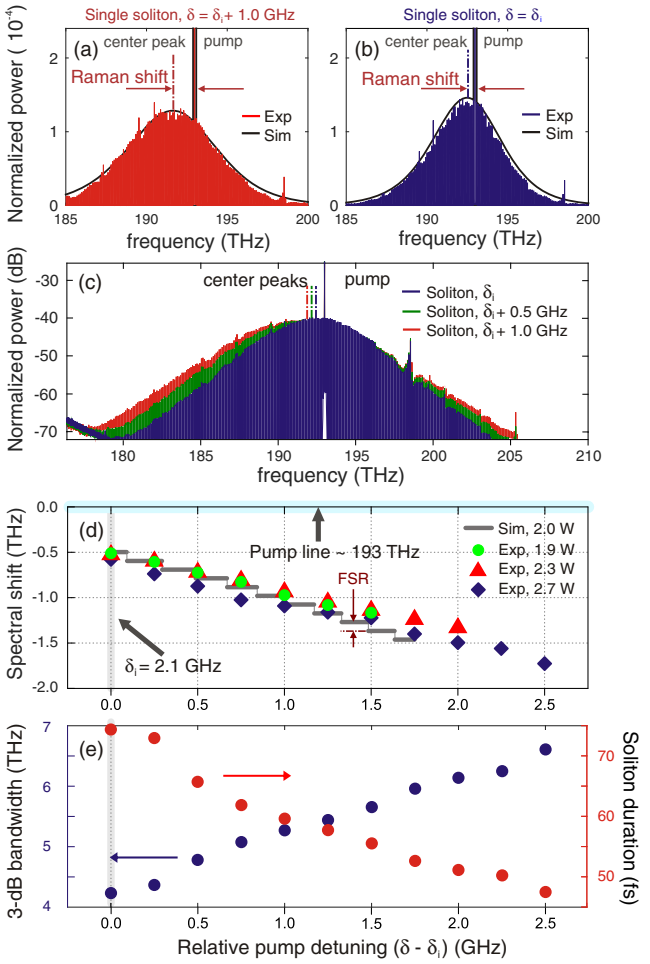

FIG. 2. (a),(b) Experimentally generated single soliton combs in a 100-GHz Si_3N_4 microresonator shown in linear scale. The envelopes are from numerical simulations. The comb power (y axis) is normalized to the cw pump power. For soliton comb simulations, we use $D_2/2\pi = 2$ MHz, $D_3/2\pi = 4$ kHz, $\kappa/2\pi = 350$ MHz, $\delta_i = 2.1$ GHz. (c) Measured soliton combs shown in logarithmic scale, the red comb [same as (a)] has $\delta = \delta_i + 1.0$ GHz, the green one $\delta = \delta_i + 0.5$ GHz, and the blue one [same as (b)] $\delta = \delta_i$. (d) Variation of the comb spectral redshift as a function of the detuning (x axis: $\delta - \delta_i$) at three pump powers: 1.9, 2.3, and 2.7 W. Note that the trend from the simulation is discrete (gray line) as we mark the specific comb line of highest power (the strong pump line excluded). Spacing corresponds to the FSR ($D_1/2\pi$). (e) Variation of the spectral 3-dB bandwidth and the (Fourier-limited) pulse duration of single temporal dissipative Kerr soliton with the pump power of 2.7 W.

[8] is a global *redshift* of the comb spectrum compared to the cw pump; cf. Fig. 2(a).

Once the single soliton state is formed, one can further explore its laser detuning dependence by tuning the pump either to red or blue wavelengths, while the soliton persists. The range of laser detuning over which the soliton state exists (i.e., the "soliton step length") here corresponds to ~2 GHz ($\sim 10 \times \kappa/2\pi$).

By choosing the blue end of the single soliton existence range as the initial detuning (δ_i), we explore the tuning

behavior of the pump wavelength over the entire soliton existence range. With an increase of the detuning, the slowly evolving comb spectrum shows two apparent trends: (1) the spectral redshift of the soliton is increased [see Figs. 2(a) and 2(b)], and (2) the spectrum is broadened, which implies soliton compression to shorter pulse duration and higher peak power [8] [Fig. 2(c)]. For comparison, a high noise frequency comb in the modulation instability (MI) operation regime is also measured (see the Supplemental Material [31]), in which the spectral redshift is absent. This is explained by the lack of coherence (phase stability of the comb modes) in this regime, which does not allow a coherent self-seeding of the comb by the stimulated Raman effects. The redshift of the comb envelope as a function of the detuning for different pump powers is shown in Fig. 2(d). We observed that the single soliton step length is enlarged with an increase in pump power. The spectral shift (ranging from 0.5 to 1.75 THz) is significant compared to the resonator's FSR (100 GHz) and exhibits a linear dependence on the laser detuning. Meanwhile, the soliton pulse duration is also tuned by the laser detuning; see Fig. 2(e). With an increase of the detuning δ the soliton is compressed from 75 to 47 fs (sub-10 cycle). Both the spectral redshift and the pulse compression are reversible and controllable.

The observed dynamics is in agreement with recent theoretical predictions by Milián *et al.* [26] who predicted a soliton redshift in dissipative Kerr solitons due to the Raman effects. In the first set of Si_3N_4 microresonators, we observed the Raman redshift on the soliton comb spectrum that is unperturbed by higher-order dispersion. Indeed, a highly symmetric comb envelope implies weak higher-order dispersion effects [e.g., soliton Cherenkov radiation (also called the dispersive wave (DW)) [36] and spectral recoil], as well as weak self-steepening effects. It is noted that the described experimental results represent (to the authors' best knowledge) the first demonstration of deterministic manipulation of the soliton self-frequency shift and soliton duration (3-dB spectrum bandwidth) in optical microresonators.

Numerical simulations.—In order to quantitatively understand the observations, we perform simulations on Kerr comb generation in Si_3N_4 microresonators based on the Lugiato-Lefever equation (LLE) [37–39]. The material Raman response is included in the LLE as a fraction of the cubic nonlinearity [26–28] (cf. Supplemental Material [31]).

We simplify the Raman response to first order for amorphous Si_3N_4, which is a reasonable approximation provided that the soliton comb bandwidth ($\Delta\omega_{3\mathrm{dB}}$) has negligible overlap with the frequency of the Raman active mode ω_R, on both positive and negative frequency axes, i.e., $\Delta\omega_{3\mathrm{dB}} < 2 \times \omega_R$. Hence, the Raman response is [40,41]

$$f_R h_R \otimes |A|^2 \approx f_R |A|^2 - f_R \tau_R \frac{\partial |A|^2}{\partial \tau}, \qquad (1)$$

where f_R indicates the Raman fraction, h_R is the Raman response function, A is the temporal envelope of the intracavity pulse, τ_R indicates the Raman shock time, and $\otimes$ denotes the convolution. Both f_R and τ_R are free parameters. The product $f_R\tau_R$ indicates the material Raman contribution on the soliton self-frequency shift.

Numerical simulations show excellent agreement to our experiments with a Raman shock time of ~20 fs (when $f_R = 20\%$) that is determined from the fit; see Fig. 2. Moreover, as independent verifications, this value is found to agree between different Si_3N_4 microresonators, including those with significantly different structural geometries. By linearly tuning δ, the comb evolution is simulated, and a transition from the noisy MI comb to soliton comb is identified. The trace of the intracavity peak power [cf. Fig. 1(c)] shows the single soliton existence range ($2\pi\delta$) from 6κ to 11κ. Figures 2(a) and 2(b) show simulated comb envelopes in the soliton state, both with significant redshifts. Simulations also verify the trend of the comb redshift as a function of the detuning δ; see Fig. 2(e).

Soliton physics and moment analysis.—In a standard cw-driven microresonator (without Raman, e.g., a crystalline resonator), the temporal dissipative Kerr soliton is understood as a self-consistent eigenpattern. This is the result of both the energy balance between the drive and the cavity loss, and the phase balance between dispersive and nonlinear effects. In the presence of material Raman effects, solitons still exist and reveal distinct behavior compared to the solitons in fiber optics where IRS continuously transfers the pulse energy from the short to long wavelength side (see the Supplemental Material [31] for detailed discussion). In microresonators, this leads to a new eigenstate of the dissipative Kerr soliton. Specifically, in the presence of the Raman effect, the energy balance is now among drive, loss, the IRS-induced pulse energy transfer, and the possible Cherenkov radiation [12] (energy shedding off from the soliton). The soliton pulse profile is consequently distorted and reveals a *fixed* amount of spectral redshift from the pump wavelength, while in optical fibers, the IRS will induce a *continuous* redshift on a local pulse that grows with propagation distance. The observed Raman-assisted stable soliton state was first numerically simulated and predicted by Milián *et al.* [26], where an asymmetric soliton pulse profile and corresponding spectrum with redshifted carrier frequency was also found (i.e., the FLR soliton). Our work further reveals that the Raman redshift is linearly tuned with the laser detuning.

To demonstrate the evolution of the soliton pulse and its independence on the propagation distance (round-trips), we simulate the intracavity pulse dynamics from the breather state to the stable soliton state, accompanied with the Raman effect. Figure 3 shows the evolution of both the pulse and spectral profiles. The detuning (δ) is fixed at the initial stage of the simulation, and there is no spectral shift being acquired over the round-trip propagation. When the detuning is linearly increased from 4κ to 9κ, the spectral redshift is also linearly increased, and the soliton continuously evolves to the stable state. Finally, if the detuning is

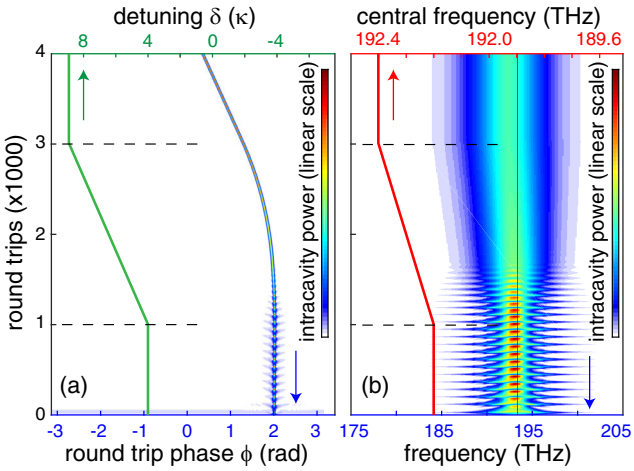

FIG. 3. (a) Simulation of a single soliton evolution from a breather state to a stable state under the change of detuning (δ). The green trace indicates the detuning and is referred to the top axis. (b) Evolution of the frequency comb spectral envelope and the Raman redshift acquired during the detuning change represented in (a). The red trace shows the central frequency of the comb envelope and is referred to the top axis.

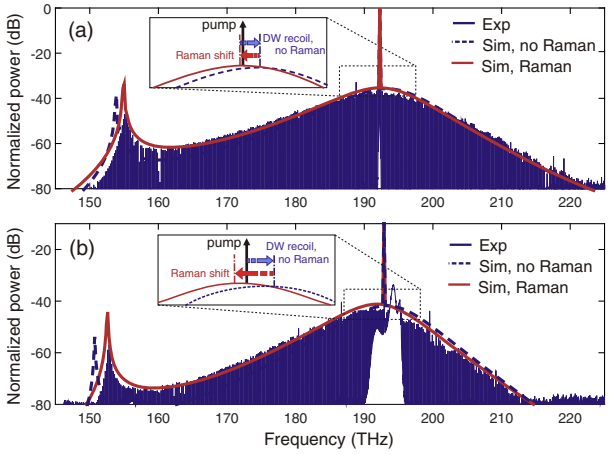

FIG. 4. Experimental generation and simulation of single soliton combs with coherent DWs in two different Si_3N_4 microresonator geometries (both having a Si_3N_4 thickness of 0.8 μm and FSR of ~190 GHz). (a) The sample with the Si_3N_4 core width of 1.8 μm (sample taken from Ref. [12]), the comb's 3-dB bandwidth is ~10 THz, $D_2/2\pi = 2.2$ MHz, $D_3/2\pi = 18$ kHz, and the fourth-order dispersion $D_4/2\pi = -350$ Hz. The pumped resonance is at 1560 nm employing 1 W of power. (b) The sample with Si_3N_4 core width of 2.0 μm, the 3-dB bandwith is ~8 THz (amplified spontaneous emission (ASE) in the EDFA is not filtered out), $D_2/2\pi = 3.2$ MHz, $D_3/2\pi = 26$ kHz, and $D_4/2\pi = -340$ Hz. The pumped resonance is at 1554 nm, the power is 1 W. Dispersion and effective mode area are calculated by finite element modeling using COMSOL, while $D_2/2\pi$ is also measured [46], showing close agreement to simulations. Blue dashed lines indicate comb envelopes without the Raman contribution.

fixed again (in the stable soliton state), previously acquired spectral shift remains unchanged.

In order to analytically investigate the Raman redshift and give a more insightful explanation, we apply the moment analysis as a perturbation method [22,42,43] to estimate the Raman effects (mainly, the first-order shock term) on the soliton dynamics in cw-driven microresonator frequency combs. The analysis treats the intracavity soliton like a particle and traces its energy, temporal position (in the microresonator), and the carrier frequency shift. In particular, the spectral redshift of the soliton is derived to be (see the Supplemental Material [31] for details)

$$\Omega_{\mathrm{CS}} \approx -\frac{64\pi^2}{15}\frac{D_1^2}{2\pi D_2}\delta f_R \tau_R, \tag{2}$$

which shows linear dependence on the laser detuning δ. The negative sign implies the carrier frequency is *redshifted*. The rate of the frequency shift is determined by the Raman shock time (in terms of $f_R\tau_R$), but is independent on the pump power. These features agree with what we observed in experiments [see Fig. 2(d)].

Cancellation of the soliton spectral recoil by the Raman shift.—We next investigate how the Raman effect influences cavity solitons in the presence of higher-order dispersion. We use two other sets of Si_3N_4 microresonators with different structural geometries that allow for shorter soliton pulses (< 30 fs) and enable coherent DW generation via the soliton-induced Cherenkov radiation process [36], as recently demonstrated in Ref. [12]. Third-order dispersion $D_3/2\pi = \mathcal{O}(10)$ kHz is characterized in the waveguide, on the fundamental TM mode. We generate single soliton combs in both samples, and, more important, a coherent DW is identified at ~155 THz. Since the DW is situated in the normal dispersion regime, the overall comb bandwidth is significantly increased to ~75 THz. The comparison of the two spectra in Figs. 4(b) and 4(c) shows the influence of the resonator dispersion on the position of the DW frequency.

It is well understood that the emission of the DW will lead to the soliton spectral recoil [36,44]. However, in the above-mentioned Si_3N_4 microresonators, the blue recoil (resulting from the DW being on the red side) was surprisingly *not* observed [12] [see Fig. 4(b)], and even a *redshift* [Fig. 4(c)] of the comb profile was seen. The explanation for this unexpected observation is that the Raman-induced soliton self-frequency shift cancels and even overcompensates the soliton blue recoil. Indeed, a similar effect has been observed in the case of soliton propagation in optical fibers [45]. We compare the two spectra to numerical simulations including both the Raman shock term and full dispersion, and we keep the previously determined value of the Raman shock time (20 fs). The simulations are again in good agreement and, in particular, reproduce the experimentally observed cancellation and overcompensation of the soliton spectral recoil by the Raman-induced redshift.

This publication was supported by Contract No. W31P4Q-14-C-0050 from the Defense Advanced Research Projects Agency, Defense Sciences Office. This

material is based upon work supported by the Air Force Office of Scientific Research, Air Force Material Command, USAF under Award No. FA9550-15-1-0099. M. K. acknowledges the support from the Marie Curie Initial Training Network FACT. V. B. acknowledges the support from the European Space Agency, European Space Research and Technology Centre. M. G. acknowledges support from both the Hasler Foundation and the "EPFL Fellows" fellowship program co-funded by Marie Curie, FP7 Grant agreement No. 291771. Si_3N_4 microresonator samples were fabricated in the EPFL Center of MicroNanotechnology (CMi).

M. K. and H. G. contributed equally to this work.

*tobias.kippenberg@epfl.ch

[1] P. Del'Haye, A. Schliesser, O. Arcizet, T. Wilken, R. Holzwarth, and T. J. Kippenberg, Nature (London) **450**, 1214 (2007).
[2] T. J. Kippenberg, R. Holzwarth, and S. Diddams, Science **332**, 555 (2011).
[3] Y. Okawachi, K. Saha, J. Levy, H. Wen, M. Lipson, and A. Gaeta, Opt. Lett. **36**, 3398 (2011).
[4] P. Del'Haye, T. Herr, E. Gavartin, M. L. Gorodetsky, R. Holzwarth, and T. J. Kippenberg, Phys. Rev. Lett. **107**, 063901 (2011).
[5] D. Moss, R. Morandotti, L. Gaeta, and M. Lipson, Nat. Photonics **7**, 597 (2013).
[6] J. Pfeifle, V. Brasch, M. Lauermann, Y. Yu, D. Wegner, T. Herr, K. Hartinger, P. Schindler, J. Li, D. Hillerkuss, R. Schmogrow, C. Weimann, R. Holzwarth, W. Freude, J. Leuthold, T. J. Kippenberg, and C. Koos, Nat. Photonics **8**, 375 (2014).
[7] J. Pfeifle, A. Kordts, P. Marin, M. Karpov, M. H. P. Pfeiffer, V. Brasch, R. Rosenberger, J. Kemal, S. Wolf, W. Freude, T. J. Kippenberg, and C. Koos, Full C and L-Band Transmission at 20 Tbit/s Using Cavity-Soliton Kerr Frequency Combs, in *CLEO: 2015 Postdeadline Paper Digest* (Optical Society of America, San Jose, CA, 2015) p. JTh5C.8.
[8] T. Herr, V. Brasch, J. D. Jost, C. Wang, M. Kondratiev, M. L. Gorodetsky, and T. J. Kippenberg, Nat. Photonics **8**, 145 (2014).
[9] S. Wabnitz, Opt. Lett. **18**, 601 (1993).
[10] N. Akhmediev and A. Ankiewicz, *Dissipative Solitons: From Optics to Biology and Medicine*, Lecture Notes in Physics (Springer, New York, 2008).
[11] T. Herr, V. Brasch, J. D. Jost, I. Mirgorodskiy, G. Lihachev, M. L. Gorodetsky, and T. J. Kippenberg, Phys. Rev. Lett. **113**, 123901 (2014).
[12] V. Brasch, T. Herr, M. Geiselmann, G. Lihachev, M. H. P. Pfeiffer, M. Gorodetsky, and T. J. Kippenberg, Science **351**, 357 (2015).
[13] X. Yi, Q. F. Yang, K. Y. Yang, M.-G. Suh, and K. Vahala, arXiv:1508.00170.
[14] Q. Lin and G. Agrawal, Opt. Lett. **31**, 3086 (2006).
[15] Y. Fu, J. Li, and C. Cao, Phys. Chem. Chem. Phys. **16**, 14808 (2014).
[16] V. Serkin, T. Belyaeva, G. Corro, and M. Granados, Quantum Electron. **33**, 325 (2003).
[17] V. Serkin, T. Belyaeva, G. Corro, and M. Granados, Quantum Electron. **33**, 456 (2003).
[18] J. Dudley, G. Genty, and S. Coen, Rev. Mod. Phys. **78**, 1135 (2006).
[19] D. V. Skryabin and A. V. Gorbach, Rev. Mod. Phys. **82**, 1287 (2010).
[20] J. Gordon, Opt. Lett. **11**, 662 (1986).
[21] N. Akhmediev, W. Krolikowski, and A. Lowery, Opt. Commun. **131**, 260 (1996).
[22] J. Santhanam and G. Agrawal, Opt. Commun. **222**, 413 (2003).
[23] A. Yulin and D. Skryabin, Opt. Lett. **31**, 3092 (2006).
[24] A. Gorbach and D. Skryabin, Opt. Express **16**, 4858 (2008).
[25] L. Yin, Q. Lin, and G. Agrawal, Opt. Lett. **32**, 391 (2007).
[26] C. Milián, A. V. Gorbach, M. Taki, A. V. Yulin, and D. V. Skryabin, Phys. Rev. A **92**, 033851 (2015).
[27] L. Zhang, Q. Lin, L. Kimerling, and J. Michel, arXiv:1404.1137.
[28] C. Bao, L. Zhang, A. Matsko, Y. Yan, Z. Zhao, G. Xie, A. Agarwal, L. Kimerling, J. Michel, L. Maleki, and A. Willner, Opt. Lett. **39**, 6126 (2014).
[29] J. Levy, A. Gondarenko, M. Foster, A. Turner-Foster, A. Gaeta, and M. Lipson, Nat. Photonics **4**, 37 (2010).
[30] M. H. P. Pfeiffer, A. Kordts, V. Brasch, C. Lecaplain, J. D. Jost, M. Geiselmann, and T. J. Kippenberg, Optica **3**, 20 (2016).
[31] See the Supplemental Material at http://link.aps.org/supplemental/10.1103/PhysRevLett.116.103902, which includes Refs. [32–35], for numerical simulation details.
[32] X. Liu, C. Xu, W. Knox, J. Chandalia, B. Eggleton, S. Kosinski, and R. Windeler, Opt. Lett. **26**, 358 (2001).
[33] R. Halir, Y. Okawachi, J. Levy, M. Foster, M. Lipson, and A. Gaeta, Opt. Lett. **37**, 1685 (2012).
[34] H. Zhao, B. Kuyken, S. Clemmen, F. Leo, A. Subramanian, A. Dhakal, P. Helin, S. Severi, E. Brainis, G. Roelkens, and R. Baets, Opt. Lett. **40**, 2177 (2015).
[35] J. Epping, T. Hellwig, M. Hoekman, R. Mateman, A. Leinse, R. Heideman, A. van Rees, P. van der Slot, C. Lee, C. Fallnich, and C. Boller, Opt. Express **23**, 19596 (2015).
[36] N. Akhmediev and M. Karlsson, Phys. Rev. A **51**, 2602 (1995).
[37] L. A. Lugiato and R. Lefever, Phys. Rev. Lett. **58**, 2209 (1987).
[38] Y. K. Chembo and C. R. Menyuk, Phys. Rev. A **87**, 053852 (2013).
[39] M. Haelterman, S. Trillo, and S. Wabnitz, Opt. Commun. **91**, 401 (1992).
[40] Y. Kodama and A. Hasegawa, IEEE J. Quantum Electron. **23**, 510 (1987).
[41] K. Blow and D. Wood, IEEE J. Quantum Electron. **25**, 2665 (1989).
[42] S. Vlasov, V. Petrishchev, and V. Talanov, Radiophys. Quantum Electron. **14**, 1062 (1971).
[43] S. Wang, H. Guo, X. Bai, and X. Zeng, Opt. Lett. **39**, 2880 (2014).
[44] M. Erkintalo, Y. Q. Xu, S. G. Murdoch, J. M. Dudley, and G. Genty, Phys. Rev. Lett. **109**, 223904 (2012).
[45] D. Skryabin, F. Luan, J. Knight, and P. Russell, Science **301**, 1705 (2003).
[46] P. Del'Haye, O. Arcizet, M. Gorodetsky, R. Holzwarth, and T. J. Kippenberg, Nat. Photonics **3**, 529 (2009).